Performance Characterization of an Active Phased Array Antenna by Simultaneously Measuring the Radiation Pattern and the Error Vector Magnitude

Máté L. Iványi[#], Gaetano Chirico[$], Yanki Aslan[#], Alexander Yarovoy[#], Marco Spirito[#]
[#]Department of Microelectronics, Delft University of Technology, The Netherlands
[$]Dipartimento di Ingegeria Elettrica e dell'Informazione, University of Cassino and Southern Lazio, Italy
m.l.ivanyi@tudelft.nl

***Abstract* — A novel over-the-air (OTA) measurement setup for simultaneous and near-real-time characterization and mapping of the phased array radiation patterns to the error-vector-magnitude (EVM) is introduced. A cost-effective software-defined radio (SDR) system, including a Pluto SDR for both transmission and reception, is employed. For setup demonstration, the performance of a 4x4 active phased array antenna (APAA) is studied at 26.5 GHz. Calibration of the transmitter results in an EVM of 0.5%, proving the accuracy of the measurement system. The over-the-air measured EVM of the APAA is 1.2%. The proposed setup and approach provide deep insights into how array radiation characteristics affect signal quality, advancing the evaluation and development of APAAs for next-generation wireless communication systems.**

***Keywords* — active phased arrays, antenna measurements, beamforming, error vector magnitude (EVM), over-the-air (OTA).**

I. Introduction

In modern millimeter-wave (mmW) communication systems (5G/6G), active phased array antennas (APAAs) are used to serve multiple users [1], [2]. One of the most significant challenges in such antenna systems is inter-beam interference (IBI) mainly caused by the high side lobes in unwanted directions. Analog beamforming circuitry, including power amplifiers (PAs) and phase shifters (PSs), also creates errors [3], and beam squinting occurs in the radiation pattern for wide bandwidths [4]. These problems, which need to be assessed and prevented, degrade the quality of the signal and thus the performance of the system [5].

One of the most commonly used metrics to assess the quality of communication systems is the signal-to-noise ratio (SNR). Traditionally, radiation pattern measurements focus on the spatial distribution of the radiated power. However, in modern wireless systems, SNR itself is not sufficient to characterize the signal quality and data-throughput rate, because it does not account for the transmitter's linearity [6]. On the other hand, bit error rate (BER) and error vector magnitude (EVM) are directly correlated with the data-throughput, and provide greater insight into the modulation performance of modern APAAs. Unlike BER, which gives only a binary information regarding the accuracy of the received data, EVM describes the error between the reference symbols and the received symbols in the complex IQ-plane, thus enabling a more detailed understanding of the linear and nonlinear distortions on the modulated signal caused by the transmitter [7].

In common practice, EVM measurements are performed in conducted setups or in an anechoic chamber with a fixed antenna orientation, while radiation pattern measurements are done separately, focusing on the antenna gain and side lobes. The mapping of radiation pattern to EVM is not a standard practice, yet there are some studies that correlate the beamforming performance with EVM through over-the-air (OTA) measurements.

In [8]–[10], far-field EVM measurements were performed of APAAs with a single receiver horn antenna. The authors in [8] and [9], experimentally investigated the dependence of EVM on the effective isotropic radiated power (EIRP) and on the beam scan angle for a single beam. At lower EIRP values, the EVM is limited by the low SNR, which is due to combined effects, i.e. the free-space path loss, the dynamic range constraints in the receiver and the noise in the transmitter and the receiver. However, at higher EIRP values, the PA nonlinearity will become the major limiting factor. In [10], a detailed analysis was performed to distinguish between the different sources of EVM contributions. It has been shown, that the EVM varies more with the scan angle at higher EIRP values than at lower EIRP values. A higher EIRP value means lower backoffs from the 1 dB compression points (P1dB) of the PAs, which result in the degradation of the beam scanning performance of the array. Furthermore, a higher modulation bandwidth result in a higher EVM value which phenomena is getting more relevant with the increase of scan angle and modulation order. Furthermore, in [11], the authors utilized a reflector antenna and a feed horn in the compact antenna test range (CATR) of the array to perform EVM measurements to reduce the free-space path loss. The input signal to the array and the output signal of the receiver horn were measured simultaneously with a vector network analyzer (VNA), thus eliminating the signal generation errors and enabling an exact comparison of the two signals. The EVM was calculated in the frequency domain by decomposing the output signal spectrum into a linear and a nonlinear frequency components by applying an equalization filter. By doing this, linear and nonlinear distortion of the CATR link could be separated in the

EVM calculation. Furthermore, the EVM contribution of each element was investigated by activating elements individually.

As seen in the literature, relevant efforts have been made to characterize the EVM performance of APAAs operating in the microwave frequency range. However, to the best of the authors' knowledge, there is no work linking radiation pattern degradations to EVM metrics. To provide new insights into the spatial impact of antenna imperfections on signal quality, a research and measurement setup is needed that can quantify how EVM varies across the entire radiation pattern, especially in the side lobe regions.

This work proposes a novel technique to experimentally investigate the direct effects of radiation pattern changes on the EVM near real-time. To this end, the Antenna Dome distributed antenna pattern OTA characterization system, which was developed at TU Delft [12], [13], is utilized, with an extension of EVM measurement capability. The rest of the paper is organized as follows. Section II describes the measurement setup, including the explanation of the data collection mechanism, the antenna under test (AUT) and the calculation of the EVM. Section III presents and discusses the measurement results. Section IV concludes the paper.

II. Measurement Setup and Characterization

A. Transmitter

The block diagram of the measurement configuration for OTA EVM measurements of an APAA is shown in Fig. 1. The digital bitstream and a Quadrature Phase Shift Keying (QPSK) waveform is generated by utilizing the Communications Toolbox Support Package for Analog Devices ADALM-Pluto Radio by MATLAB running on a PC, which is the central control unit of the measurement setup. The digital waveform is sent to a cost-effective software-defined radio (SDR) through a USB cable. The SDR utilized in the setup is an Analog Devices ADALM-PLUTO [14] module operating in the 325 MHz - 3.8 GHz frequency range. It has two RF channels, enabling simultaneous transmitting and receiving. The IF signal generated by the SDR is sent to an upconverter to convert the signal to the mmW frequency range. The upconverted signal is connected to the AUT

B. Antenna Under Test (AUT)

The AUT is a 4 × 4 APAA from TMYTEK [15], which is operated at 26.5 GHz. It has 16 controllable RF channels connected to patch antennas. Each channel offers 360° phase control with 5° steps, and 15 dB attenuation range with 0.5 dB steps. RMS phase and attenuation errors are 4° and 0.35 dB, respectively. In transmit mode, it achieves an EIRP of 41.5 dBm. Its control is facilitated via an SPI interface for SDR integration. The included TMXLAB software enables intuitive UI and API-based phase and amplitude control for efficient beam steering.

C. Antenna Dome and 3D Pattern Acquisition

Unlike traditional scanning equipment with mechanical control, the multiple fixed-probe Dome system (shown in Fig. 2) significantly reduces measurement time while compromising the pattern resolution [12]. The current configuration consists of 35 dual-polarized nodes and a boresight receiver probe antenna linked to a downconverter for EVM measurements. These components are strategically placed at the joints of aluminum profiles and within the anechoic panels of the geodesic dome. Absorbing panels are placed around the dome, mimicking an anechoic environment. The lowest node is positioned at 26.2° elevation, with the boresight node at 90°, and all nodes are located 75 cm from the AUT, ensuring far-field measurements at 26.5 GHz. Each node includes two orthogonally arranged sensing units and a readout board. The sensing units use broadband Vivaldi antennas with a 14 dBi gain at 26.5 GHz and contain an RMS power meter and a 12-bit analog-to-digital converter (ADC) [13]. This setup enables rapid power pattern acquisition (under 10 ms) in both co- and cross-polarization without requiring complex RF cabling. The measured power data and the interpolated 3D radiation pattern can be processed using MATLAB scripts. Additional details on the Dome are available in previous studies [12], [13].

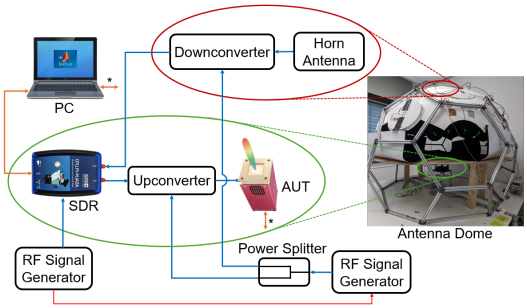

Fig. 1. Measurement setup for simultaneous OTA EVM and radiation pattern measurements. (RF signals are shown in blue, reference signals in red, and control signals in orange. Signal paths marked with a star also indicate direct connections.)

Fig. 2. AUT pattern measurements in the Antenna Dome.

D. Boresight Receiver and EVM Characterization

The downconverter is connected to the boresight receiver horn antenna and positioned outside the shielding panels. The LO signal for the up- and down-conversion is produced by a single RF signal generator to ensure the right power levels to the mixers and synchronization. The downconverted signal is received by the SDR, which uses an external clock from

another signal generator. The two signal generators and so the whole system is synchronized by the 10 MHz reference signal. Finally, digital signal processing is done by the PC.

As mentioned in Section I, EVM quantifies the combined effects of linear and nonlinear amplitude and phase distortions in the received modulated signal arising from the transmitter circuitry together with the antenna elements, which makes the EVM an informative performance metric for APAAs. Conventionally, the EVM is defined as the root mean square (RMS) average value of the error vectors between the reference and the measured set of symbols at the receiver, as shown in (1):

$$EVM(\%) = \frac{\sqrt{\frac{1}{N}\sum_{i=1}^{n} |x(t_i) - e(t_i)\cdot y(t_i)|^2}}{\sqrt{\frac{1}{N}\sum_{i=1}^{n} |x(t_i)|^2}} \times 100 \quad (1)$$

where the input signal, the received signal and the equalization filter, compensating for phase rotation, group delay and frequency dispersion are denoted by $x(t_i)$, $y(t_i)$ and $e(t_i)$, respectively. The expression in (1) is based on demodulation with a vector signal analyzer (VSA) of the received signal. This methodology, however, can be ineffective for modern wide-band digital signals due to the high memory size and processing capability demands and that generator noise and matching inaccuracies significantly decrease the dynamic range of the EVM measurement. To overcome these issues, a new technique was proposed in [16] for PAs which was extended to APAAs in [11]. This technique is based on measuring the input and output spectrum by a vector network analyzer (VNA) instead of a VSA and estimating the EVM in the frequency domain instead of the time domain, eliminating the need of different test signals and complex demodulation processes. The expression in (2) from [16] can be derived from (1) by applying Parseval's theorem:

$$EVM(\%) = \frac{\sqrt{\frac{1}{N}\sum_{i=1}^{n} |X(f_i) - E(f_i)\cdot Y(f_i)|^2}}{\sqrt{\frac{1}{N}\sum_{i=1}^{n} |X(f_i)|^2}} \times 100 \quad (2)$$

where $X(f_i)$, $Y(f_i)$ and $E(f_i)$ are the spectrum of the input signal, the output signal and the equalization filter, respectively.

The proposed approach eliminates the need for expensive measurement equipment, such as VNAs or VSAs, while ensuring synchronization by utilizing a single cost-effective SDR for both transmission and reception. The EVM calculation with an equalization filter is performed after down-sampling in the digital domain, ensuring high dynamic range and fast acquisition of the EVM. Furthermore, having two separate but synchronized compact boards for the upconverter and the downconverter makes it possible to attach the downconverter on the top of the Antenna Dome, and reducing cable loss in the high-frequency region. By putting the AUT inside the Antenna Dome, fast acquisition of the radiation pattern can be done simultaneously with the EVM measurements which give valuable insights on the relations between the two.

III. Measurement Results

Firstly, the transmitter was characterized to obtain its contribution to EVM. To this end, a digital waveform was generated in MATLAB using QPSK modulation applied to 1000 random bits. The signal was then upsampled and filtered with a root-raised-cosine filter having a roll-off factor of 0.25, and then connected to the SDR. The SDR, operating at a sample rate of 40 MHz and a carrier frequency of 3.5 GHz, was continuously transmitting the QPSK modulated signal which, after upconversion and filtering at 26.5 GHz, was directly connected back to the receiver. Fig. 3 shows the power spectrum of the transmitted waveform at the output of the transmitter.

To compensate for random errors, 100 QPSK frames were received and averaged. Furthermore, systematic errors were calibrated out by applying the inverse of the transfer function, which serves as an equalization filter to the averaged signal. Fig. 4 shows the bathtub curve of the EVM versus power level before and after calibration. Different power levels at the transmitter output were achieved by varying the transmit gain of the Pluto. It can be seen from the figure that the calibrated EVM has a wide flat part from -38 to -6 dBm, where the EVM remains below 2%.

After characterizing the performance of the transmitter by conducted measurements, the proposed measurement setup (see Fig. 1) was utilized to charaterize the AUT. It can be seen from Fig. 5 that the EVM of the AUT was improved after calibration. Below -35 dBm of input power, the noise, while above -12 dBm, the nonlinear behavior of the amplifiers degrades the EVM. Between the two, the EVM remained

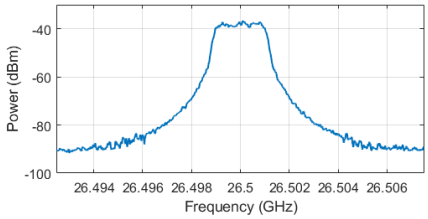

Fig. 3. Power spectrum of the transmitter waveform.

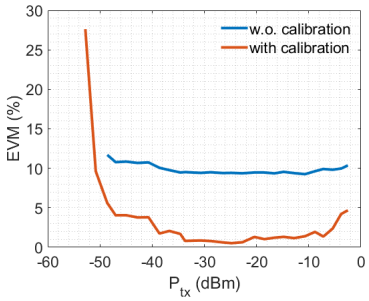

Fig. 4. Conducted bathtub curve of the EVM versus transmit power level before and after calibration.

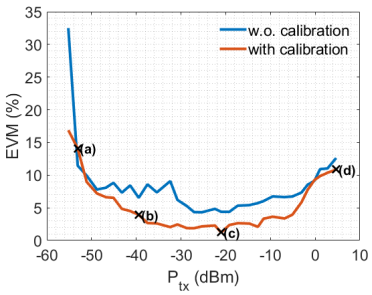

Fig. 5. OTA measured bathtub curve of the EVM versus transmit power level before and after calibration.

stable between 1% and 3%. Fig. 6 shows the received constellation diagrams with the corresponding OTA EVM values for different transmit power levels for the boresight beam. The labels (a)-(d) refer to the corresponding points in Fig. 5. Fig. 7 illustrates the measured pattern examples with interpolation.

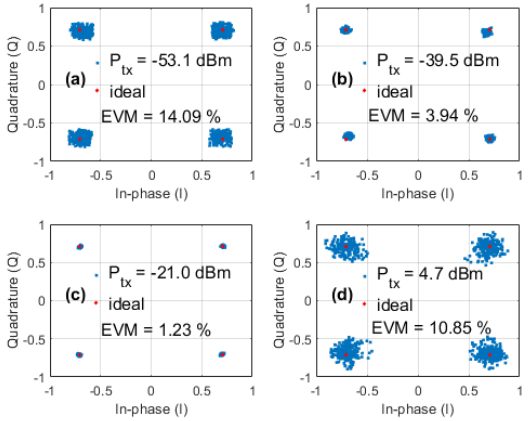

Fig. 6. OTA received QPSK constellation diagrams and EVM values for different transmit power levels.

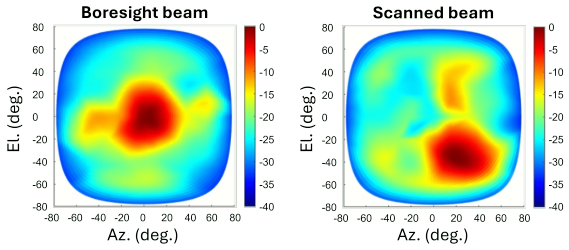

Fig. 7. Examples of normalized and interpolated radiation patterns (in dB) of the AUT measured in the Antenna Dome.

IV. Conclusion

A novel technique to experimentally investigate the direct effects of radiation pattern changes on the EVM near real-time is proposed. To this end, the Antenna Dome, a distributed antenna pattern OTA characterization system is utilized and expanded with EVM measurement capability. The experimental verification of the proposed technique is performed. The OTA EVM performance characterization of the AUT is shown while measuring the radiation pattern simultaneously for varying scan angles.

Acknowledgment

This research was supported by the National Growth Fund through the Dutch 6G flagship project “Future Network Services”.

References

[1] X. Gu, D. Liu, and B. Sadhu, “Packaging and antenna integration for silicon-based Millimeter-Wave phased arrays: 5G and beyond,” *IEEE Journal of Microwaves*, vol. 1, no. 1, pp. 123–134, 2021.

[2] W. Hong, Z. H. Jiang, C. Yu, *et al.*, “The role of Millimeter-Wave technologies in 5G/6G wireless communications,” *IEEE Journal of Microwaves*, vol. 1, no. 1, pp. 101–122, 2021.

[3] Y. Aslan, P. Aubry, N. B. Onat, J. Janssen, M. Geurts, and A. Yarovoy, “Heuristic over-the-air calibration of beamformer ics in active mm-wave phased arrays,” in *2023 IEEE Conference on Antenna Measurements and Applications (CAMA)*, 2023, pp. 840–845.

[4] M. Y. Javed, N. Tervo, M. E. Leinonen, and A. Pärssinen, “Wideband inter-beam interference cancellation for mmW/sub-THz phased arrays with squint,” *IEEE Transactions on Vehicular Technology*, vol. 72, no. 6, pp. 7560–7572, 2023.

[5] Y. Aslan, J. Puskely, A. Roederer, and A. Yarovoy, “Trade-offs between the quality of service, computational cost and cooling complexity in interference-dominated multi-user sdma systems,” *IET Communications*, vol. 14, no. 1, pp. 144–151, 2020.

[6] D. Brown and Y. Rahmat-Samii, “Error vector magnitude as a performance standard for antennas in the millimeter-wave era: Part 1: Metric comparisons and measurement concepts,” *IEEE Antennas and Propagation Magazine*, vol. 65, no. 5, pp. 25–34, 2023.

[7] D. Brown and Y. Rahmat-Samii, “Error vector magnitude as a performance standard for antennas in the millimeter-wave era: Part 2: Modeling, simulation, and measurement methods,” *IEEE Antennas and Propagation Magazine*, vol. 65, no. 6, pp. 10–24, 2023.

[8] Y. Yin, S. Zihir, T. Kanar, *et al.*, “A 37–42-GHz 8 × 8 phased-array with 48–51-dBm EIRP, 64–QAM 30-Gb/s data rates, and EVM analysis versus channel RMS errors,” *IEEE Transactions on Microwave Theory and Techniques*, vol. 68, no. 11, pp. 4753–4764, 2020.

[9] A. Bagheri, H. Karlsson, C. Bencivenni, *et al.*, “TX beamforming EVM performance of a 65 dBm-EIRP slant-polarized gapwaveguide phased array at 28 GHz,” in *2023 17th European Conference on Antennas and Propagation (EuCAP)*, 2023, pp. 1–4.

[10] S. Spira, K. Blau, R. Thomä, and M. A. Hein, “5G mm-Wave over-the-air measurements of an agile multi-beam front-end,” in *2020 50th European Microwave Conference (EuMC)*, 2021, pp. 153–156.

[11] D. Brown and Y. Rahmat–Samii, “Compact antenna test range EVM measurements of a Millimeter-Wave phased array using a VNA,” in *2022 IEEE International Symposium on Phased Array Systems & Technology (PAST)*, 2022, pp. 01–05.

[12] F. A. Musters, R. Coesoij, M. Migliore, F. Schettino, and M. Spirito, “The antenna dome real-time distributed antenna pattern characterization system,” in *2021 97th ARFTG Microwave Measurement Conference (ARFTG)*, 2021, pp. 1–5.

[13] R. A. Coesoij, F. A. Musters, D. Roos, T. van Velden, and M. Spirito, “Calibration approaches in multi-node antenna characterization setups,” in *2023 100th ARFTG Microwave Measurement Conference (ARFTG)*, 2023, pp. 1–4.

[14] A. Devices, *Adalm-pluto sdr active learning module*, https://www.analog.com/media/en/news-markettingcollateral/product-highlight/ADALM-PLUTO-Product-Highlight.pdf, 2017.

[15] TMY Technology Inc., *BBox One 5G 28 GHz datasheet*, version V1.0.12, Datasheet for BBox One 5G 28 GHz, sold by NI. Part numbers: 788823-01 (standard), 788826-01 (academic)., National Instruments Corp., 2022. [Online]. Available: https://www.ni.com.

[16] J. Verspecht, A. Stav, J.-P. Teyssier, and S. Kusano, “Characterizing amplifier modulation distortion using a vector network analyzer,” in *2019 93rd ARFTG Microwave Measurement Conference (ARFTG)*, 2019, pp. 1–4.